Applied Science and Innovative Research
ISSN 2474-4972 (Print) ISSN 2474-4980 (Online)
Vol. 9, No. 4, 2025
www.scholink.org/ojs/index.php/asir

Original Paper

Optimization of Structural Parameters for UAV Spray Nozzles Using Response Surface and Genetic Algorithms

Yujie Li[1], Qingzheng Liu[2] & Chaojie Zhai[3]

[1,2,3] School of Mechanical Engineering, Shaanxi University of Technology, Hanzhong, Shaanxi, 723001, China

Received: October 18, 2025 Accepted: November 17, 2025 Online Published: November 24, 2025

doi:10.22158/asir.v9n4p81 URL: http://doi.org/10.22158/asir.v9n4p81

Abstract

A fan-shaped nozzle for unmanned aerial vehicle spraying was designed to investigate the influence of three key parameters—nozzle outlet diameter, relative cutting depth, and groove angle—on outlet velocity and pressure drop. Using a central composite design (CCD) with 20 sample points, numerical simulation methods were employed to solve for outlet velocity and pressure drop. A response surface model linking outlet diameter, relative cutting depth, and groove angle to outlet velocity and pressure drop was constructed using Kriging. A multi-objective genetic algorithm was applied to optimize structural parameters, targeting maximum outlet velocity and minimum pressure drop. The optimal structural parameters were determined as: outlet diameter 3.0 mm, relative cutting depth 1.2 mm, and groove angle 120.0°. Compared to the original prototype, this configuration achieved a 15.7% increase in outlet velocity and a 7.8% reduction in pressure drop.

Keywords

Numerical simulation, CCD experiment, Response surface model

1. Introduction

High-voltage line insulators play a critical role in power transmission systems, with their performance directly impacting the safe and stable operation of the power grid (Zhang Nan, Zheng Chengshi, & He Xiaojuan, 2018). In recent years, rapid technological advancements and the demands of social productivity have led to the emergence of drone spraying as a novel tool for power system maintenance. Compared to traditional manual maintenance methods—which are inefficient, costly, and hazardous—drone spraying offers the advantages of high efficiency and low cost, playing a significant role in power maintenance. The spray nozzle, as the working tip of the spraying drone, directly influences performance metrics such as coating coverage, atomization angle, and spray uniformity. Within the drone spraying

system, the nozzle structure is the primary determinant of spraying performance, affecting coating uniformity and ultimately coating quality. Existing research by domestic and international experts focuses on optimizing spray nozzle structures.

Structural optimization involves adjusting key parameters such as nozzle aperture size, relative cutting depth, and groove angle to systematically enhance core performance metrics including flow stability, atomization angle precision, and distribution uniformity. Fan-shaped nozzle optimization represents a particularly prominent example. Dongling Y. et al. (2021) analyzed the dry granulation and atomization characteristics of zirconia using the VOF (Volume of Fluid) method, then further investigated the impact of different nozzle diameters. The study found that increasing the nozzle outlet diameter from 3 mm to 4 mm enhanced the liquid jet velocity and widened the spray angle, while the liquid film thickness decreased. However, when the nozzle outlet diameter expanded to 5 mm, the liquid ejection velocity decreased, the spray angle narrowed further, and the liquid film thickness continued to diminish. Yue, Y. S., Chen, G. J., and Chen, C. (2019) employed the VOF method to analyze the effects of nozzle diameter, inlet chamfer, and back pressure on atomization characteristics. Results indicate: as nozzle diameter increases, flow rate decreases and diesel injection velocity reduces, but atomization range expands; as nozzle inlet chamfer angle increases, diesel injection velocity uniformly increases while injection flow rate, velocity, and atomization range also expand; as back pressure increases, internal nozzle pressure rises, but back pressure's impact on atomization characteristics remains relatively minor. Pan Huachen, Zhou Zelei, and Liu Lei. (2017) investigated the influence of nozzle structural parameters on atomization characteristics through numerical simulation. Results indicate: variations in groove position and angle affect spray particle size and atomization angle; the tangential groove inclination angle significantly impacts atomization angle—greater inclination yields narrower atomization angles; increasing pressure reduces particle diameter while widening atomization angle.

Existing nozzle designs have achieved certain results, but in the field of drone spraying, limitations such as low atomization efficiency and difficulty in controlling droplet drift necessitate the development of novel nozzle designs. This involves investigating how nozzle structure influences spraying performance to determine the optimal configuration. This paper designs a nozzle structure for spraying drones, explores how structural parameters affect the internal flow field, and identifies the optimal structural parameters.

2. Materials and Methods

2.1 Structure and Parameters of Drone Spraying Equipment

2.1.1 Drone Spraying System

As shown in Figure 1, the drone spraying system primarily consists of two components: the drone and the spraying equipment. The drone mainly comprises the drone body (1) connected to the propeller (2), forming an assembly with the landing gear (3) below. The spraying equipment connects to the drone via a pod (7) and primarily consists of a spray boom (4), spray nozzles (5), a material tank (6), and a water

pump inside the tank.

The operational sequence is as follows: Prior to takeoff, the coating material is loaded into the tank. Upon reaching the target area, the pump activates to convey the coating through the spray boom to the nozzle, which then sprays the material onto the designated zone. After completion, the pump shuts off, and the drone initiates its return flight, departing the target area. It lands smoothly at the designated landing point using its landing gear.

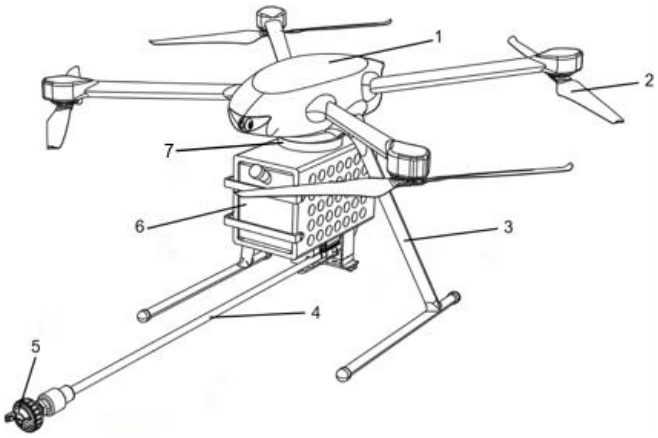

Figure 1. Structure of Spray Unmanned Aerial Vehicle

1. Unmanned Aerial Vehicle (UAV) 2. Propeller 3. Landing Gear 4. Spray Boom 5. Spray Nozzle 6. Material Hopper 7. Pod

Throughout the spraying process, the nozzle structure significantly influences the velocity and pressure distribution within the nozzle flow field, thereby affecting spray performance (Liu Juan, Sun Mingbo, Li Qinglian, et al., 2011; Wang Shuai., 2021; Sun Mingbo, Li Qinglian, et al., 2011; Yu Haoyang, Liu Aiguo, Chen Si, et al., 2020; Zhang Hongsheng, Guan Tianxiang, & Liu Haizhou., 2020; Wang Chao, & Yao Jie., 2016; Gao Wei., 2023; Gao Xueqing, Wang Ding, Li Xinde, et al., 2023; Li Ruimin, Xu Chao, Chen Yongcheng et al., 2014). Among these, three structural parameters—spray nozzle outlet diameter, relative cutting depth, and cutting groove angle—are the primary determinants of internal flow field characteristics. As documented (Bai, B. P., Xing, M. Y., & Wang, Z., 2014) in the current range of structural parameters for spray nozzles on spraying drones is: outlet diameter 0.5~5 mm, cutting groove angle 30~120°, and relative cutting depth 0.2~1.2 mm, as shown in Table 1.

Table 1. Range of Structural Parameters

Parameter Name	Parameter Range
Grooving angle	30 ~ 120°
Relative cutting depth	0.3 ~ 1.2mm
Outlet diameter	2 ~ 3mm

The three-dimensional model of the drone spraying nozzle is shown in Figure 2. It primarily comprises three structural parameters: outlet diameter, relative cutting depth, and groove angle. This paper uses a fan-shaped atomizing nozzle with an outlet diameter D of 2.5 mm, a groove angle α of 30°, and a relative cutting depth Hr of 0.6 mm as the original sample.

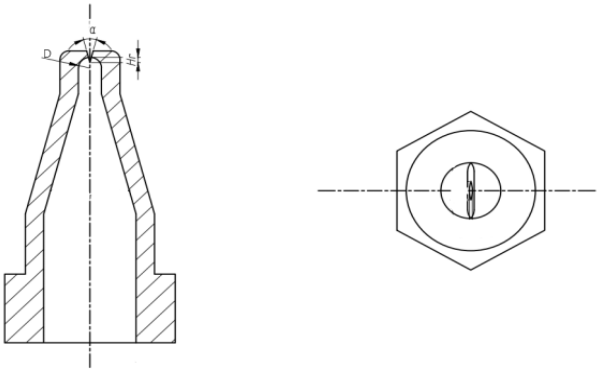

Figure 2. Planar Structure Diagram of the Spray Head

2.1.2 Structural Parameter Optimization Process

The technical workflow for structural parameter optimization is shown in Figure 3.

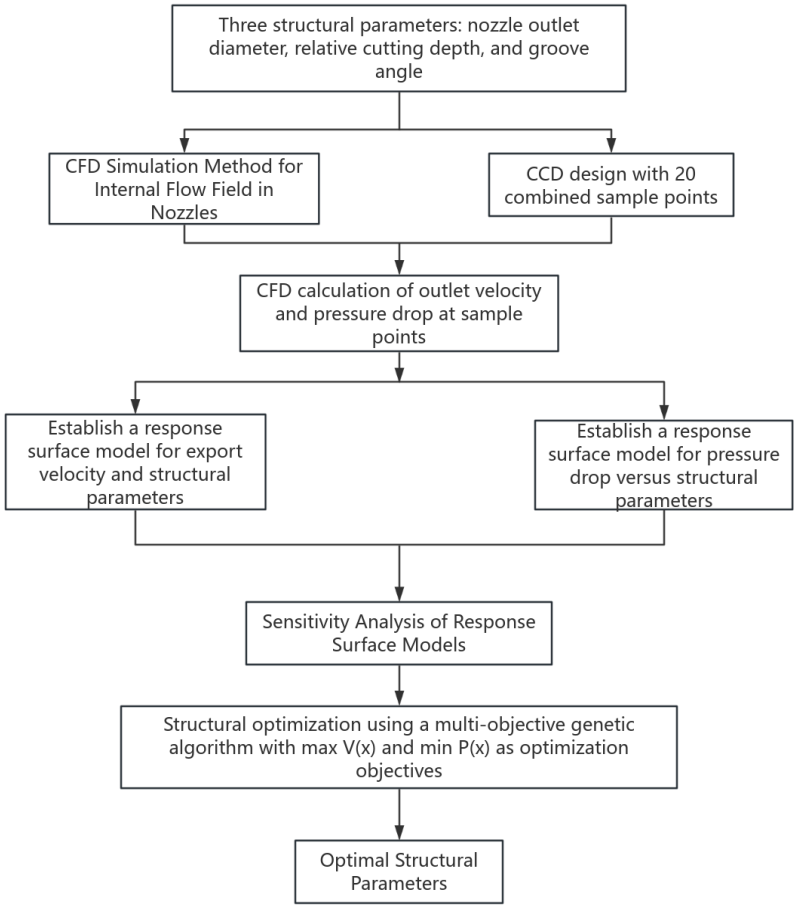

Figure 3. Flow Chart of Structural Parameter Optimization

This paper optimizes three structural parameters of the drone spray nozzle: outlet diameter, relative cutting depth, and groove angle. A CCD central composite design was employed to generate 20 sample points for the combination of these parameters. CFD simulations calculated the outlet velocity and pressure drop at each sample point, followed by sensitivity analysis on the response surface model. Polynomial regression was employed to establish response surface models linking outlet velocity and pressure drop to each structural parameter. With the objectives of maximizing outlet velocity and minimizing pressure drop, a multi-objective genetic algorithm was applied to optimize the structural parameters, yielding the optimal configuration.

2.2 Numerical Simulation Methods for Internal Flow Fields

A hybrid mesh (hexahedral + tetrahedral) was employed to partition the fluid domain, with local refinement near walls to capture flow details, achieving high mesh quality. The mesh configuration is shown in Figure 4. The fluid domain comprises 1,794,019 mesh cells and 313,451 mesh nodes. All cells within the fluid domain exhibit a quality factor exceeding 0.5, with an average skew ratio above 0.9.

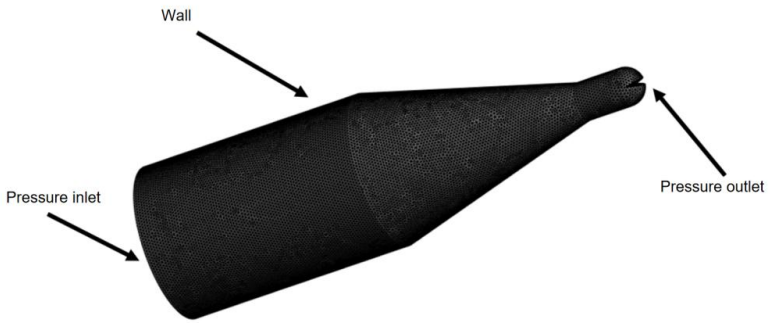

Figure 4. Rendering of Mesh Division

Fluent was employed to solve for nozzle outlet velocity and pressure drop. The internal flow medium was water-based polyurethane paint with a density of 1300 kg/m³ and viscosity of 0.05 kg/(m·s). The turbulence model used was the RNG k-ε model, suitable for numerical simulation of high Reynolds number internal flows and capable of accurately capturing turbulent flow characteristics. Gravitational effects on flow were neglected. The inlet pressure ranged from 200,000 to 1,000,000 Pa, while the outlet pressure was set to standard atmospheric pressure. Solutions were obtained using the first-order upwind scheme and the Coupled scheme.

A set of nozzle samples was constructed under three parameter combinations: outlet diameter, relative cutting depth, and cutting groove angle. Fluent was employed to solve for the outlet velocity and pressure drop of these nozzle samples as the working pressure increased from 200,000 Pa to 1,000,000 Pa.

2.3 Combined Sample Point Design and Model Construction Method

2.3.1 Combined Sample Point Design

A central composite design was employed to construct experimental sample points for the nozzle under three parameter combinations: outlet diameter, relative cutting depth, and groove angle. Building upon a

three-factor full-level experiment, this design expanded each factor to five levels by introducing repeated central and axial points, thereby meeting the requirements for response surface model fitting. Based on the three structural parameters—inlet diameter, relative cutting depth, and groove angle—the CCD method was employed to construct 20 experimental sample points. These included 8 cubic points, 6 axial points containing α-level extreme points, and 6 central points for repeated experiments, as shown in Figure 5.

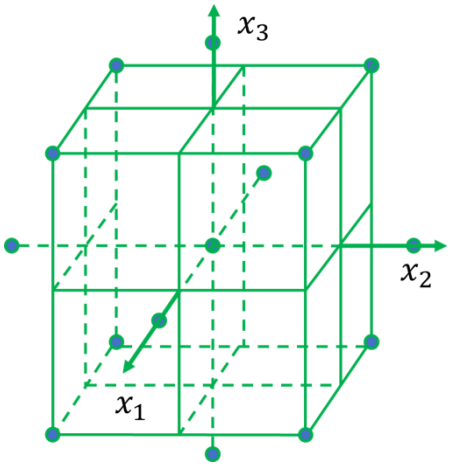

Figure 5. Central Composite Design

2.3.2 Response Surface Construction Method

By constructing 20 sample points for outlet diameter, relative cutting depth, and groove angle versus outlet velocity and pressure drop through CCD center combination experiments, a response surface model linking structural parameters to outlet velocity and pressure drop was established using Kriging. Its mathematical expression is as follows:

$$y(x) = \boldsymbol{f}^{\mathrm{T}}(x)\beta + z(x)$$

In the formula: $f^{\mathrm{T}}(x)$ It is a quadratic polynomial of the design parameter x and serves as the global approximation model. β The basis function coefficients in the surrogate model; $z(x)$ has an expected value of 0, Variance is σ^2, and obeys a Gaussian random function that follows a normal distribution. $z(x)$ Possesses the following statistical properties:

$$E[z(x)] = 0$$

$$Var[z(x)] = \sigma_z^2$$

$$Cov[z(x_i), z(x_j)] = \sigma^2[R_{ij}(\theta, x_i, x_j)] \cdots i, j = 1,2, \cdots n$$

In the formula: x_i and x_j are any two input variables.; $R_{\tilde{y}}(\theta, x_i, x_i)$is a function related to parameter $\boldsymbol{\theta}$;

The accuracy of the model is determined by the stochastic process $z(x)$, whose expression is :

$$R_{ij}(\theta, x_i, x_j) = \exp\left(-\sum_{k}^{n_m} \theta_k \left|x_k^i - x_k^j\right|^2\right)_{\nu}$$

In the formula: n_m is the number of random variables; The kth component corresponding to x_i、x_j is x_k^i and x_k^j ; θ_k is the correlation parameter, determined by maximum likelihood estimation of the correlation function, i.e.,

$$\theta = \min\left[(\det R)^{\frac{1}{m}}\sigma^2\right]$$

For a given set of input variables $X = [x_1, x_2, \cdots, x_n]$ and its corresponding set of responses $Y = [y_1, y_2, \cdots, y_n]$, The estimated value of β and σ^2 are

$$\hat{\beta} = (F^{\mathrm{T}}R^{-1}F)^{-1}F^{\mathrm{T}}R^{-1}Y_\omega$$

$$\hat{\sigma}^2 = \frac{(Y - F\hat{\beta})^T R^{-1}(Y - F\hat{\beta})}{n}$$

In the formula: $\hat{\beta}$ and $\hat{\sigma}^2$ are the estimated values of β and σ^2, respectively; $\boldsymbol{r}(x)$ Correlation function vector between prediction points and sample points;

Finally, the predicted response value for the unknown point x is obtained through the Kriging model as

$$\hat{y}(x) = \hat{\beta} + \boldsymbol{r}^{\mathrm{T}}(x)R^{-1}\left(\mathbf{Y} - \mathbf{f}\hat{\beta}\right)^{\omega}.$$

$$\boldsymbol{f} = [f(x_1), f(x_2), \cdots, f(x_n)]^T,$$

$$r(x) = [R(x, x_1), R(x, x_2), \cdots, R(x, x_n)]^T$$

In the formula: $\hat{y}(x)$ Predicted values for sample points; $\mathbf{r}^{\mathrm{T}}(x)\mathbf{R}^{-1}\left(\mathbf{Y} - \mathbf{f}\hat{\beta}\right)$ Interpolation for the surrogate model.

2.4 Multi-Objective Genetic Algorithm

Higher outlet velocity achieves superior atomization, while lower pressure drops results in reduced energy loss and more stable flow output. These objectives present a trade-off during nozzle structural optimization. Therefore, based on the constructed response surface model, a multi-objective genetic algorithm is employed to perform global optimization targeting both maximum outlet velocity and minimum pressure drop, thereby determining the optimal structural parameters.

Multi-objective genetic algorithm for nozzles is:

$$\max \mathrm{V(x)} = [\mathrm{V_1(x), V_2(x), \cdots, V_n(x),}]$$

$$\min \mathrm{P(x)} = [\mathrm{P_1(x), P_2(x), \cdots, P_n(x),}]$$

$$\begin{cases} \mathrm{n} = 1,2,\cdots,\mathrm{N} \\ \mathrm{H_i(x)} \le \mathrm{H_0(x)} \\ \mathrm{G_j(x)} \ge \mathrm{G_0(x)} \\ \mathrm{x} = [\mathrm{x_1, x_2, \cdots, x_d, \cdots, x_D}] \\ \mathrm{x_{dmin}} \le \mathrm{x_d} \le \mathrm{x_{dmax}} \quad \mathrm{d} = 1,2,3,4 \\ \mathrm{i} = 1,2,\cdots,\mathrm{m;\ j} = 1,2,\cdots,\mathrm{k} \end{cases}$$

In the formula: x is a structural parameter; $\mathrm{m, n, i, j, d}$ is the number of states for the variable; $\mathrm{x_d}$ is the structural parameter range; $\mathrm{V(x)}$ is the output speed; $\mathrm{P(x)}$ represents the voltage drop.

The solution process of the Multi-Objective Genetic Algorithm (MOGA) is based on a population iteration optimization mechanism: First, an initial population is generated. Subsequently, the fitness of individuals is evaluated based on the constructed response surface model, and valid solutions are

screened through constraint conditions. The screened individuals undergo genetic recombination to generate a new population, with the process iterating cyclically until convergence criteria are met. This process continuously optimizes the dual objective function of outlet velocity and pressure drop, ultimately outputting the optimal individuals that maximize outlet velocity and minimize pressure drop. These represent the optimal solutions for the three structural parameters: outlet diameter, relative cutting depth, and cutting groove angle. The algorithm initially generates 3000 samples, producing 600 samples per iteration, and identifies 3 candidate samples within a maximum of 20 iterations.

3. Results and Analysis

3.1 Relationship between Structural Parameters and Outlet Velocity and Pressure Drop

3.1.1 Relationship between Structural Parameters and Outlet Velocity

The nozzle outlet velocity primarily depends on structural parameters such as outlet diameter, relative cutting depth, and groove angle. Establish velocity variation curves for each structural parameter under different pressures.

At an inlet pressure of 200,000 Pa, the relationship between outlet diameter and velocity is shown in Figure 6. As the outlet diameter increases from 2.0 to 2.2 mm, the nozzle outlet velocity rises sharply; As the outlet diameter increases from 2.2 to 2.5 mm, the outlet velocity increases rapidly; As the outlet diameter increases from 2.5 to 2.8 mm, the outlet velocity increases slowly; As the outlet diameter increases from 2.8 to 3.0 mm, the outlet velocity increases rapidly. The maximum outlet velocity of 24.8 m/s is achieved at an outlet diameter of 3.0 mm.

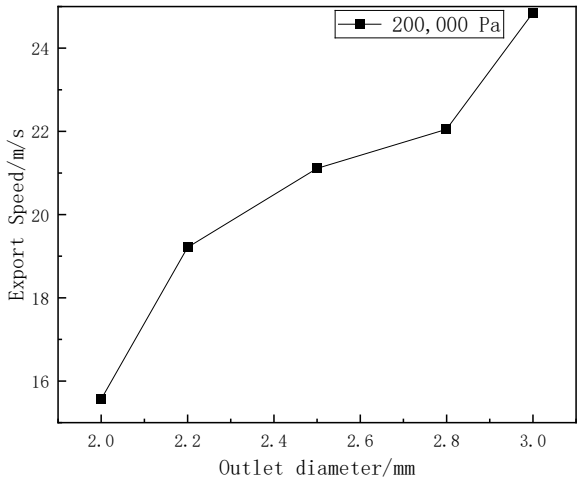

Figure 6. Curve of the Relationship between Outlet Diameter and Outlet Velocity at 200000Pa

The outlet velocity and outlet diameter of the nozzle, along with the velocity variation curve under different pressures, are shown in Figure 7. As the inlet pressure increases from 200,000 Pa to 1,000,000 Pa, the outlet velocity also increases. At an inlet pressure of 1,000,000 Pa, the nozzle achieves its maximum outlet velocity.

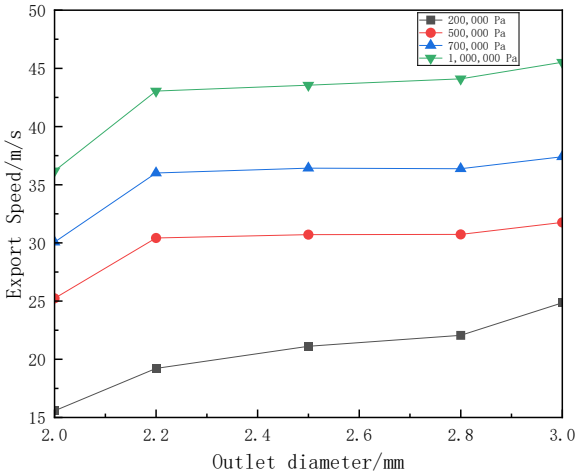

Figure 7. Curves of the Relationship between Outlet Diameter and Outlet Velocity under Different Pressures

Figure 8 shows the variation curve of relative cutting depth versus outlet velocity at an inlet pressure of 200,000 Pa. When the relative cutting depth varies within the range of 0.3 to 0.48 mm, the nozzle outlet velocity initially increases slowly. After the relative cutting depth exceeds 0.48 to 0.75 mm, the outlet velocity shifts to a rapid increase. Beyond 0.75–1.02 mm, the outlet velocity exhibits a steep increase trend; when the relative cutting depth exceeds 1.02–1.2 mm, the outlet velocity again increases rapidly. At a relative cutting depth of 1.2 mm, the nozzle outlet velocity reaches its maximum value of 23.1 m/s.

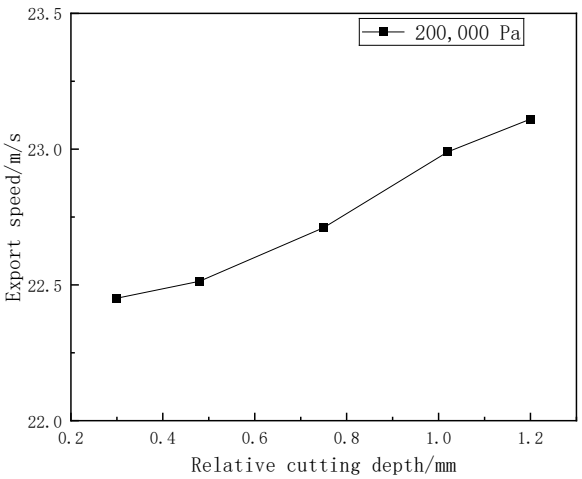

Figure 8. Curve of the Relationship between Relative Cutting Depth and Outlet Velocity at 200000Pa

Figure 9 shows the variation curve of the nozzle outlet velocity with inlet pressure, as a function of the relative cutting depth and outlet diameter. As the inlet pressure increases from 200,000 Pa to 1,000,000 Pa, the outlet velocity also increases. The maximum outlet velocity is achieved at an inlet pressure of 1,000,000 Pa.

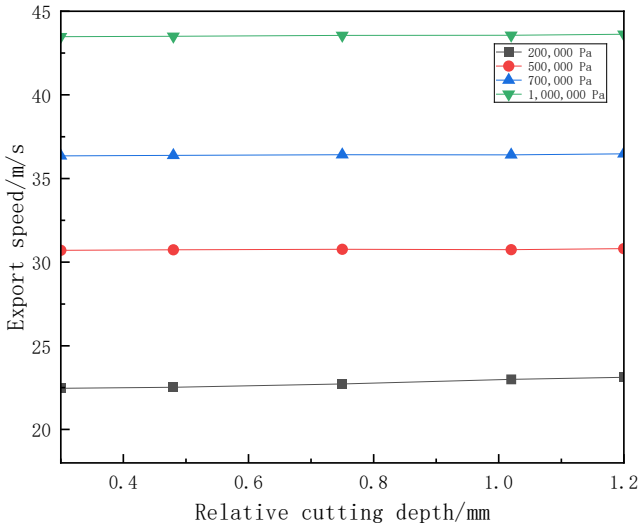

Figure 9. Curves of the Relationship between Relative Cutting Depth and Outlet Velocity under Different Pressures

Figure 10 shows the variation curve of the outlet velocity with the cutting angle when the inlet pressure is 200,000 Pa. As the slot angle varied between 30° and 120°, the nozzle outlet velocity exhibited a continuous increasing trend. At a slot angle of 75°, the outlet velocity increased rapidly. At a slot angle of 101.2°, the outlet velocity surged sharply. At a slot angle of 120°, the outlet velocity reached its maximum value of 28.0 m/s.

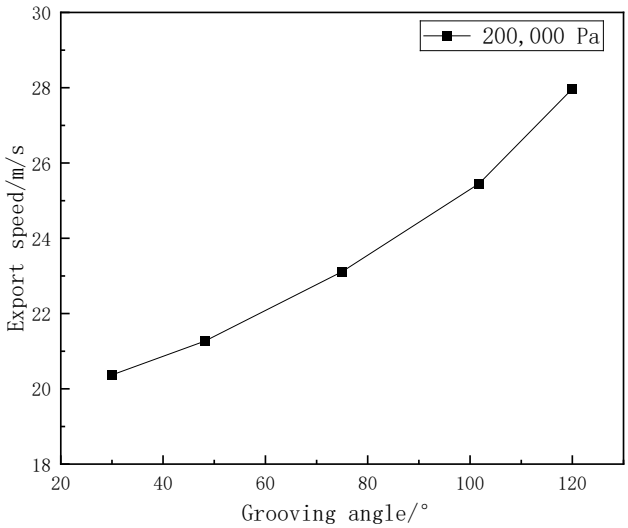

Figure 10. Curve of the Relationship between Groove Depth and Outlet Velocity at 200000Pa

Figure 11 shows the variation curve of outlet velocity with inlet pressure for the nozzle's slot angle and outlet diameter. As the inlet pressure increases from 200,000 Pa to 1,000,000 Pa, the outlet velocity rises accordingly. The nozzle achieves its maximum outlet velocity at an inlet pressure of 1,000,000 Pa.

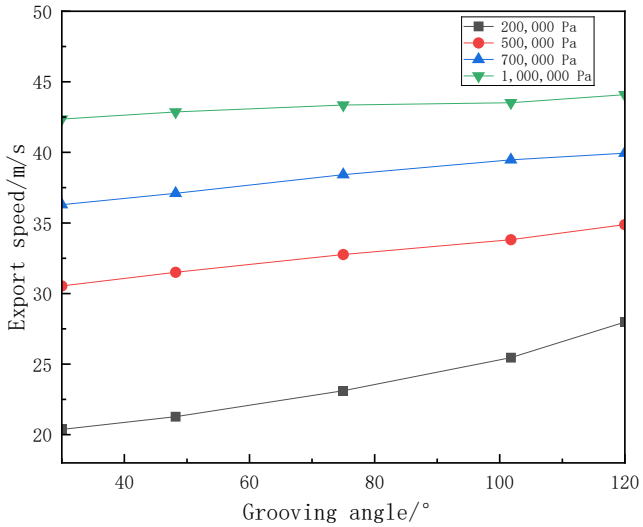

Figure 11. Curves of the Relationship between Groove Depth and Outlet Velocity under Different Pressures

3.1.2 Relationship between Structural Parameters and Pressure Drop

The pressure drop curve as a function of outlet diameter at an inlet pressure of 200,000 Pa is shown in Figure 12. Within the outlet diameter range of 2.0 to 3.0 mm, the nozzle's pressure drop first decreases slowly, then drops sharply, followed by another slow decrease before dropping rapidly again. At an outlet diameter of 3.0 mm, the nozzle's pressure drop reaches its minimum value of 192,191 Pa.

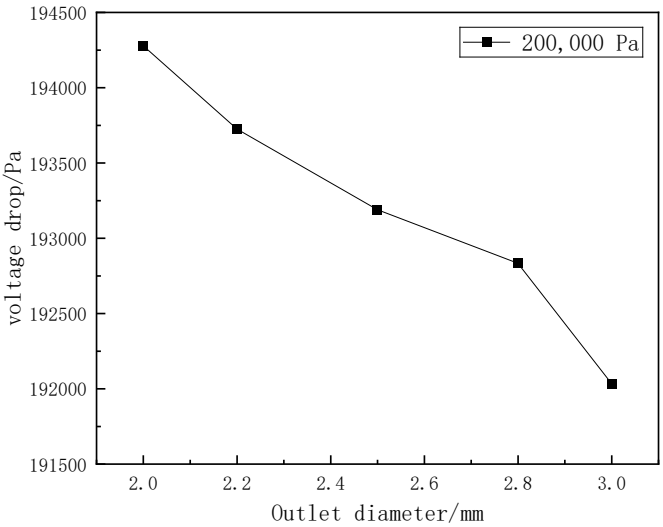

Figure 12. Curve of the Relationship between Outlet Diameter and Pressure Drop at 200000Pa

Figure 13 shows the pressure drop variation curve with outlet diameter under different inlet pressures. As the inlet pressure increases from 200,000 Pa to 100,000 Pa, the pressure drop also increases. The nozzle exhibits the minimum pressure drop at an inlet pressure of 200,000 Pa.

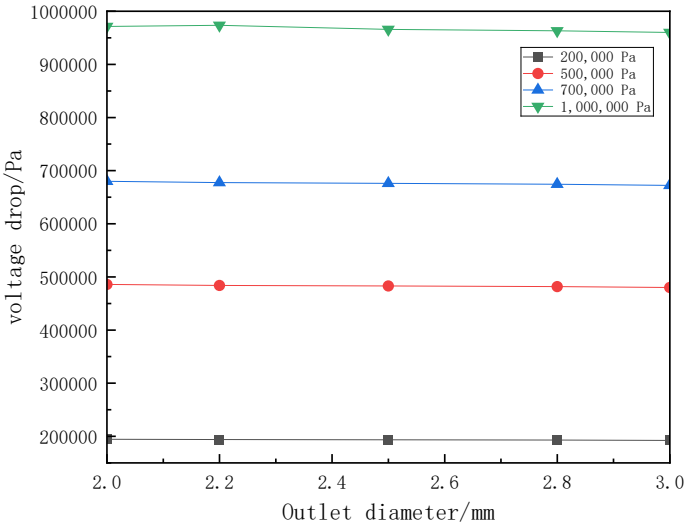

Figure 13. Curves of the Relationship between Outlet Diameter and Pressure Drop under Different Pressures

The variation curve of relative cutting depth with pressure drop at an inlet pressure of 200,000 Pa is shown in Figure 14. Within the range of 0.3 to 1.2 mm relative cutting depth, the nozzle pressure drop first decreases slowly, then rapidly, followed by a steep decline and a subsequent gradual decrease. At a relative cutting depth of 1.2 mm, the nozzle pressure drop reaches its minimum value of 188,325 Pa.

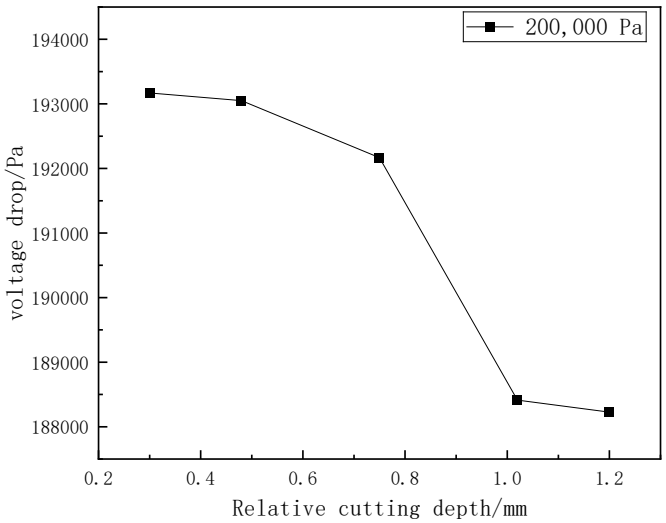

Figure 14. Curve of the Relationship between Relative Cutting Depth and Pressure Drop at 200000Pa

Figure 15 shows the pressure drop variation curve with outlet diameter under different inlet pressures. As the inlet pressure increases from 200,000 Pa to 100,000 Pa, the pressure drop also increases. The nozzle exhibits the minimum pressure drop at an inlet pressure of 200,000 Pa.

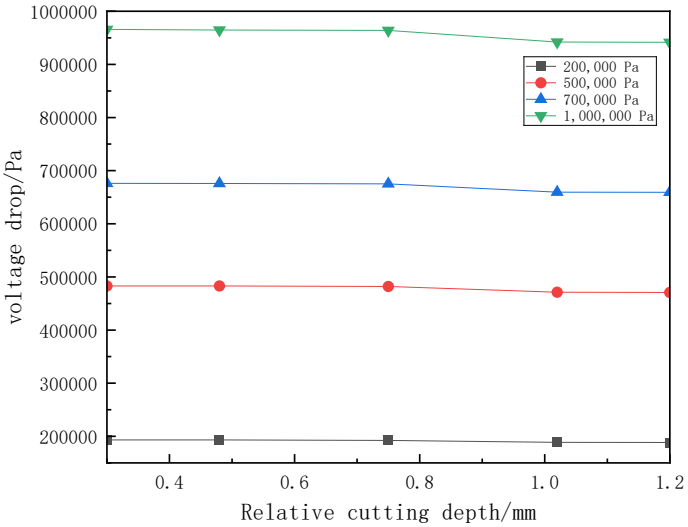

Figure 15. Curves of the Relationship between Relative Cutting Depth and Pressure Drop under Different Pressures

The variation curve of the slot angle with pressure drop at an inlet pressure of 200,000 Pa is shown in Figure 16. Within the slot angle range of 30° to 120°, the nozzle's pressure drop exhibits a continuous and gradual downward trend. At a slot angle of 120°, the nozzle's pressure drop reaches its minimum value of 192,064 Pa.

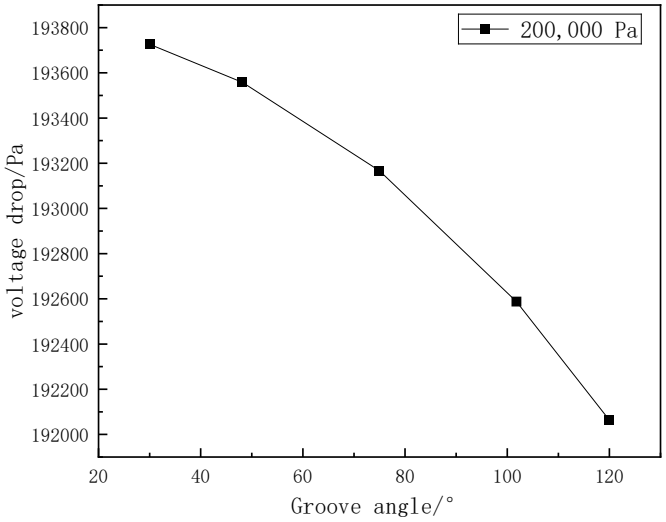

Figure 16. Curve of the Relationship between Groove Depth and Pressure Drop at 200000Pa

Figure 17 shows the pressure drop variation curve with outlet diameter under different inlet pressures. As the inlet pressure increases from 200,000 Pa to 100,000 Pa, the pressure drop also increases. The nozzle exhibits the minimum pressure drop at an inlet pressure of 200,000 Pa.

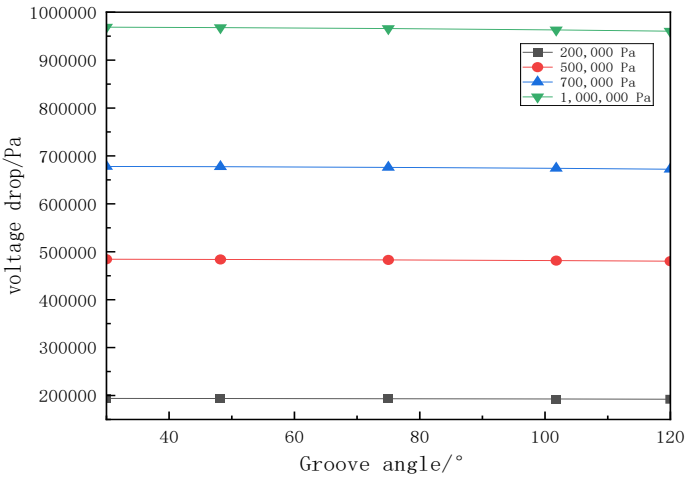

Figure 17. Curves of the Relationship between Groove Depth and Pressure Drop under Different Pressures

3.2 Response Surface Modeling and Sensitivity Analysis

Using Fluent software and the Kriging method, response surface equations were constructed for the three structural parameters—outlet diameter (x1), relative cutting depth (x2), and groove angle (x3)—in relation to outlet velocity and pressure drop. Sensitivity analysis of the structural parameters was performed based on these response surface equations. Higher sensitivity indicates a more significant influence of the structural parameter on performance, as shown in Figure 18.

Regarding outlet velocity, outlet diameter exhibits a positive effect; relative cutting depth shows a strong positive effect; and cutting angle demonstrates a weak positive effect. In terms of sensitivity, the order is (positive) > (strong positive) > (weak positive).

Regarding pressure drop, outlet diameter exhibits a negative effect; relative cutting depth shows a strong negative effect; and groove angle demonstrates a weak negative effect. Sensitivity follows the order: (strong negative) > (negative) > (weak negative).

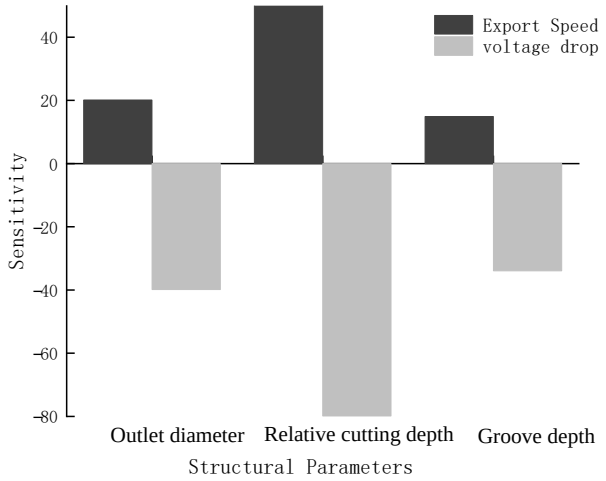

Figure 18. Sensitivity of Structural Parameters

3.3 Optimal Structural Parameters

With maximum outlet velocity and minimum pressure drop as objective functions, MOGA was employed to globally optimize structural parameters. An initial population was constructed using a screening method, and response surface modeling was applied to calculate outlet velocity and pressure drop, as shown in Figure 19. Three sets of optimal structural parameters were obtained, as listed in Table 2. The optimized models achieved an average 15.62% increase in outlet velocity and a 6.94% reduction in pressure drop compared to the original prototype. Comparing the three optimized models, Optimization Point 3 exhibited the highest outlet velocity and lowest pressure drop. Therefore, point 3 was selected as the final model in this study.

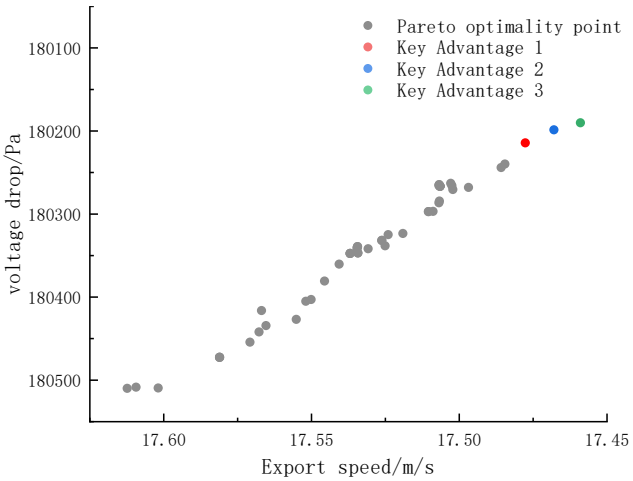

Figure 19. Sensitivity of Structural Parameters

Table 2. Optimal Structural Parameters

Parameters	Original parameter value	Point 1	Point 2	Point 3
Outlet diameter/ mm	2.5	2.9989	2.9973	2.9974
Relative cutting depth/ mm	0.6	1.1997	1.1995	1.1998
Grooving angle/ (°)	30.0	119.96	119.85	119.72
Export Speed/(m/s)	15.11	17.47	17.46	17.48
Pressure Drop/Pa	195388.52	185063.14	180214.12	180200.38
Export Speed Optimization Ratio/ %		15.62	15.55	15.68
Pressure Drop Optimization Ratio/ %		-5.28	-7.76	-7.77

For machining convenience, the final optimal structural parameters for the single group are: outlet diameter 3.0 mm, relative cutting depth 1.2 mm, and groove angle 120.0°. This configuration achieves an outlet velocity of 564.8 m/s and a pressure drop of 185,063.1 Pa.

4. Results and Analysis

1) A response surface model was constructed for structural parameters versus outlet velocity and pressure drop. Key sensitivity analysis indicates: For outlet velocity, outlet diameter exhibits a positive effect; relative cutting depth shows a strong positive effect; while the groove angle exhibits a weak positive effect. Sensitivity ranking: $x_2 > x_1 > x_3$. For pressure drop: outlet diameter shows a negative effect; relative cutting depth exhibits a strong negative effect; groove angle shows a weak negative effect. Sensitivity ranking: $x_2 > x_1 > x_3$.

2) The outlet velocity increases rapidly with increasing outlet diameter before slowing down, increases significantly with increasing relative cutting depth before stabilizing, and increases approximately linearly with increasing groove angle. The pressure drop decreases approximately linearly with increasing relative cutting depth/outlet diameter and decreases slightly with increasing groove angle.

3) Optimal structural parameters determined via multi-objective optimization: outlet diameter 3.0 mm, relative cutting depth 1.2 mm, and groove angle 120.0°. Compared to the original prototype, this configuration achieves a 15.7% increase in outlet velocity and a 7.8% reduction in pressure drop.

Funding Project

General Project of the Shaanxi Provincial Department of Science and Technology (2022JM-131).

References

Bai, B. P., Xing, M. Y., & Wang, Z. (2014). Experiment Study and Simulation Research for the Atomization Characteristics of the Internal-Mixing Twin-Fluid Atomizer. *Advanced Materials Research*, *3593*(1049-1050),1075-1082.

Dongling, Y., Zuoxiang, Z., Jiangen, Z., et al. (2021). Influence of nozzle outlet diameter on the atomization process of zirconia dry granulation. *Advances in Mechanical Engineering*, *13*(6), 16878140211024885-16878140211024885.

Gao Wei. (2023). Design and Simulation of Structural Parameters for Spray Nozzles in Crop Protection Drones Based on SolidWorks and ANSYS. *Agricultural Technology and Equipment*, *2023*(08), 40-42.

Gao Xueqing, Wang Ding, Li Xinde, et al. (2023). Structural Optimization of Centrifugal Atomizing Nozzles and Droplet Deposition Characteristics. *Journal of Irrigation and Drainage Machinery Engineering*, *41*(07), 749-756.

Li Ruimin, Xu Chao, Chen Yongcheng et al. (2014). Research and Analysis of Key Parameters for Fan-Shaped Spray Nozzles. *Agricultural Mechanization Research*, *000*(012), 208-211.

Liu Juan, Sun Mingbo, Li Qinglian, et al. (2011). Analysis of the Influence of Centrifugal Nozzle Structural Parameters on Performance Based on the VOF Method. *Journal of Aerodynamics*, *26*(12), 2826-2833. https://doi.org/10.13224/j.cnki.jasp.2011.12.016

Pan Huachen, Zhou Zelei, & Liu Lei. (2017). Study on the Influence of Key Structural Parameters on the Atomization Effect of Centrifugal Atomizing Nozzles. *Transactions of the Chinese Society for Mechanical Engineering*, *53*(02), 199-206.

Sun Mingbo, Li Qinglian, et al. (2011). Analysis of the Influence of Centrifugal Nozzle Structural Parameters on Performance Based on the VOF Method. *Journal of Aerodynamics*, *26*(12), 2826-2833. https://doi.org/10.13224/j.cnki.jasp.2011.12.016

Wang Chao, & Yao Jie. (2016). Design Research on Multi-Nozzle Paint Vacuum Atomization Spraying Chamber. *Science and Technology Outlook*, *26*(24), 171.

Wang Shuai. (2021). *Study on Atomization Characteristics and Particle Size Analysis of Fan-Shaped Nozzles*. Jiangsu University.

Yu Haoyang, Liu Aiguo, Chen Si, et al. (2020). Study on the Influence of Structural Parameters on the Atomization Characteristics of Pneumatic Atomizing Nozzles. *Journal of Shenyang Aerospace University*, *37*(05), 1-9.

Yue, Y. S., Chen, G. J., & Chen, C. (2019). Influence of nozzle structure parameters on atomization characteristics. *Energy Engineering*.

Zhang Hongsheng, Guan Tianxiang, & Liu Haizhou. (2020). Optimization of Spray Nozzle Structure for Spray Robots. *Light Industry Machinery*, *38*(05), 99-102.

Zhang Nan, Zheng Chengshi, & He Xiaojuan. (2018). Discussion on Relay Protection Failures and Countermeasures in 110kV Substations. *Engineering Technology Research*, *2018*(15), 65-66.